

# Theoretical and Experimental Study of Sawtooth Effect in Isolated Cardiac Cell-Pairs

VINOD SHARMA, PH.D., and LESLIE TUNG, PH.D.

From the Department of Biomedical Engineering, The Johns Hopkins University, Baltimore, Maryland

**Sawtooth Effect in Cell-Pairs. Introduction:** The question of how a defibrillation shock affects the myocardium far ( $> \sim 1$  mm; the space constant of continuum tissue models) from the electrode is not fully understood. According to a long-standing, yet to be verified, hypothesis, the relatively high-resistance intercellular gap junctions may help in coupling the shock effect to the distant myocardium by redistributing the defibrillation current and creating a sawtooth pattern of polarization in which every cell undergoes hyperpolarization and depolarization. The goal of this study was to conduct an in-depth theoretical and experimental investigation of the sawtooth effect in the simplest coupled system, that of an isolated cell-pair.

**Methods and Results :** Theoretically, we present a relationship between sawtooth amplitude (STA) and junctional resistance ( $R_j$ ), and show that, in a cell-pair with two cells of different lengths, the sawtooth effect may not necessarily appear as a reversal in polarization across the junction when  $R_j$  is below a critical value. Experimentally, we optically mapped transmembrane potential responses along the lengths of enzymatically isolated guinea pig cell-pairs at 10- or 17- $\mu$ m resolution, and estimated STA as the magnitude of discontinuity in responses at the intercellular junction. From 14 cell-pairs, STA was estimated to be  $\sim 11$  mV for a nominal 10 V/cm field. Based on our theoretical results, this value corresponds to an  $R_j$  of  $\sim 18$  M $\Omega$ .

**Conclusion:** The intercellular junction induces a measurable sawtooth effect in the simplest system of an isolated cell-pair. An accounting for the sawtooth effect might be essential for understanding field-tissue interaction far from the electrode and to accurately predict tissue response during field stimulation. (*J Cardiovasc Electrophysiol*, Vol. 12, pp. 1164-1173, October 2001)

*transmembrane potential, voltage-sensitive dye, optical mapping, junctional resistance*

## Introduction

Despite the widespread clinical use of defibrillation shocks, the basic mechanisms by which a shock terminates fibrillation in a heart are yet to be fully understood. Experimentally, it has been established that the shock must affect the myocardium distant (many centimeters) from the electrode to be successful.<sup>1-3</sup> However, mechanisms by which shock affects the distant myocardium are not completely clear. Originally, the structural complexities of the cardiac tissue were not appreciated, and it was thought to be a homogeneous continuum (core conductor or bidomain) medium. Such representation of cardiac tissue can explain *surface polarization* only, with shock effects extending at most to a few millimeters into the bulk of the myocardium.<sup>4</sup> However, it is now known that heterogeneities such as fiber branching<sup>5</sup> and changes in fiber direction,<sup>5-7</sup> intercellular clefts,<sup>8</sup> and spatial variations in intracellular and extracellular volumes<sup>9</sup> can all potentially play a role in tissue polarization far from the electrode. Among these plausible mechanisms to explain field-tissue interaction in the bulk of the myocardium is the hypothesis put forth by Plonsey and

Barr.<sup>10</sup> Based on their theoretical work with field stimulation of linear cell strands, they suggested that periodic resistive discontinuities introduced by the intercellular gap junctions may redistribute the defibrillation current, resulting in a sawtooth pattern of polarization in which every cell undergoes depolarization and hyperpolarization at its two ends. Subsequently, other simulation studies in one-dimensional,<sup>11-13</sup> two-dimensional (2-D),<sup>13-15</sup> and three-dimensional (3-D)<sup>16</sup> models of passive or active myocardium have produced qualitatively similar results. However, the staggered arrangement of cells in 2-D, and presumably 3-D, myocardium can act to depress the sawtooth amplitude (STA).<sup>13,14</sup>

Experimentally, the sawtooth effect has been well characterized in the limiting case of a single cell.<sup>17-20</sup> Single-site<sup>17,19</sup> and multisite<sup>18,20</sup> optical mapping studies of cells stimulated with uniform fields have revealed a nonuniform polarization of the cell in which the cell end facing the cathode undergoes maximum depolarization and the end facing the anode undergoes maximum hyperpolarization, with polarization varying monotonically along the cell length.<sup>18,20</sup> However, few studies have investigated whether the sawtooth effect is preserved in multicellular structures in which the cells are interconnected via finite resistance intercellular connections. Gillis et al.<sup>21</sup> optically recorded field responses at subcellular resolution from cultured monolayers of neonatal myocytes and failed to observe a significant change, much less an abrupt reversal, in polarization across the intercellular junctions. In another study, Zhou et al.<sup>22</sup> used a double-barrel microelectrode technique to record field responses from guinea pig papillary muscle.

This work was supported by National Institutes of Health Grant HL48266 and a Johns Hopkins Independent Research Grant.

Address for correspondence: Leslie Tung, Ph.D., Department of Biomedical Engineering, The Johns Hopkins University, 720 Rutland Avenue, Baltimore, MD 21205. Fax: 410-955-0549; E-mail: ltung@bme.jhu.edu

Manuscript received 14 March 2001; Accepted for publication 11 August 2001.

By sequentially recording from sites separated by 20  $\mu\text{m}$  over a 0.4-mm tissue length, they sought a reversal in polarity of the responses between any two adjacent sites, but they also were unsuccessful. In both of these studies, the investigators concluded that the intercellular junctions do not induce a measurable sawtooth effect. These two studies have been commonly cited by others as evidence against the sawtooth hypothesis.

Undoubtedly, the pattern of polarization of cells within a syncytial network is influenced by cell-cell interactions across intercellular junctions. For instance, for a cell-pair with very high intercellular resistance, the two cells can be considered as isolated cells, and a maximum STA can be expected at the intercellular junction. On the other hand, when the intercellular resistance is low enough so that the cell-pair behaves like a single supercell, STA is expected to be zero, while the polarization at the opposite ends of the cell-pair is maximized. There is ample experimental evidence to support the notion that the resistance of the junctional region that spans only 0.5 to 2  $\mu\text{m}$  of the cell length<sup>23</sup> is comparable to the total intracellular resistance of the entire cell.<sup>24-27</sup> Thus, any two interconnected cells in the myocardium are unlikely to behave as a supercell, and a complete absence of sawtooth effect as suggested by Gillis et al.<sup>21</sup> and Zhou et al.<sup>22</sup> is difficult to reconcile with the theory.

The aim of this study was to characterize the sawtooth effect theoretically and experimentally via high-resolution optical mapping in the simplest coupled system, that of an isolated cell-pair. We derive an analytical expression for STA in a cell-pair with variable intercellular resistance that is subjected to a uniform field stimulus. We also present results from high-resolution optical mapping of transmembrane responses from adult guinea pig ventricular cell-pairs. A careful examination of the data reveals the presence of the sawtooth effect.

### Theoretical

Consider two cells of lengths  $L_1$  (cell 1) and  $L_2$  (cell 2) connected with a variable intercellular resistance ( $R_j$ ) at an intercellular junction located at the origin ( $x = 0$ ). Furthermore, let the diameter  $d$  of each cell be 20  $\mu\text{m}$ , the typical average diameter of a guinea pig ventricular cell.<sup>28</sup> In response to an externally applied field ( $E_o$  in the  $+x$  direction), the steady-state transmembrane voltage  $V_m$  for each cell is the solution of the following differential equation<sup>29</sup> subject to the appropriate boundary conditions:

$$\lambda^2 \frac{d^2 V_m}{dx^2} - V_m = 0 \quad (1)$$

where  $\lambda = \sqrt{r_m/r_i}$  is the space constant. This definition of  $\lambda$  holds when  $r_e \ll r_i$ , where  $r_i$  and  $r_e$  are the intracellular and extracellular resistances per unit length (in  $\Omega/\text{cm}$ ), respectively, and  $r_m = R_m/\pi d$ , where  $R_m$  is the membrane specific resistance. The intracellular current  $I_i$  can be related to  $V_m$  and  $E_o$  by Equation 2:

$$I_i = -\frac{1}{r_i} \frac{d\phi_i}{dx} = -\frac{1}{r_i} \frac{d}{dx} [V_m + \phi_e] = -\frac{1}{r_i} \frac{dV_m}{dx} + \frac{E_o}{r_i} \quad (2)$$

where  $\phi_i$  and  $\phi_e$  are the intracellular and extracellular potentials, respectively. In arriving at Equation 2, the rela-

tions  $V_m = \phi_i - \phi_e$  and  $E_o = -d\phi_e/dx$  were used. To solve Equation 1, we use the following boundary conditions:

1. Sealed nonjunctional ends of the cell-pair, i.e.,  $I_i = 0$  at  $x = -L_1$  and  $x = +L_2$
2. Continuity of  $I_i$  at the intercellular junction, i.e.,  $I_i|_{x=0^-} = I_i|_{x=0^+}$
3. Applicability of Kirchhoff's voltage law at the junction, i.e.,  $V_m|_{x=0^-} - V_m|_{x=0^+} = I_i R_j$ .

The  $V_m$  for the two cells is given by:

$$V_m = \begin{cases} \frac{2E_o}{\kappa} \left[ \alpha \sinh \left( \frac{x + \frac{L_1 - L_2}{2}}{\lambda} \right) + \beta_1 \sinh \left( \frac{x + \frac{L_1}{2}}{\lambda} \right) \right] & (3A) \\ \frac{2E_o}{\kappa} \left[ \alpha \sinh \left( \frac{x + \frac{L_1 - L_2}{2}}{\lambda} \right) + \beta_2 \sinh \left( \frac{x - \frac{L_2}{2}}{\lambda} \right) \right] & (3B) \end{cases}$$

where

$$\alpha = \lambda \sinh \left( \frac{L_1 + L_2}{2\lambda} \right) \quad (4A)$$

$$\beta_1 = \frac{R_j}{r_i} \sinh \left( \frac{L_1}{2\lambda} \right) \sinh \left( \frac{L_2}{\lambda} \right) \quad (4B)$$

$$\beta_2 = \frac{R_j}{r_i} \sinh \left( \frac{L_1}{\lambda} \right) \sinh \left( \frac{L_2}{2\lambda} \right) \quad (4C)$$

$$\kappa = \sinh \left( \frac{L_1 + L_2}{\lambda} \right) + \frac{R_j}{\lambda r_i} \sinh \left( \frac{L_1}{\lambda} \right) \sinh \left( \frac{L_2}{\lambda} \right). \quad (4D)$$

The details of the derivation are given in the Appendix.

### Two Cells of Equal Length

If both cells are of equal length  $L$ , the constants  $\alpha$ ,  $\beta_1$ ,  $\beta_2$ , and  $\kappa$  in Equations 4A to 4D can be simplified and Equations 3A and 3B reduce to Equations 5A and 5B:

$$V_m = \begin{cases} \frac{2E_o}{\kappa_s} \left[ \lambda \sinh \left( \frac{x}{\lambda} \right) + \beta_s \sinh \left( \frac{x + \frac{L}{2}}{\lambda} \right) \right] & x < 0 \quad (5A) \\ \frac{2E_o}{\kappa_s} \left[ \lambda \sinh \left( \frac{x}{\lambda} \right) + \beta_s \sinh \left( \frac{x - \frac{L}{2}}{\lambda} \right) \right] & x > 0 \quad (5B) \end{cases}$$

where

$$\beta_s = \frac{R_j}{r_i} \sinh(L/2\lambda) \quad \text{and} \quad (6A)$$

$$\kappa_s = 2 \cosh(L/\lambda) + \frac{R_j}{\lambda r_i} \sinh(L/\lambda). \quad (6B)$$

In the limiting case when  $R_j = 0$ , Equations 5A and 5B reduce to Equation 7, and when  $R_j \rightarrow \infty$ , they reduce to Equations 8A and 8B:

$$V_m = \frac{\lambda E_o}{\cosh(L/\lambda)} \sinh(x/\lambda) \quad R_j = 0, \text{ all } x \quad (7)$$

$$V_m = \begin{cases} \frac{\lambda E_o}{\cosh(L/2\lambda)} \sinh\left(\frac{x + \frac{L}{2}}{\lambda}\right) & R_j \rightarrow \infty, x < 0 \quad (8A) \\ \frac{\lambda E_o}{\cosh(L/2\lambda)} \sinh\left(\frac{x - \frac{L}{2}}{\lambda}\right) & R_j \rightarrow \infty, x > 0. \quad (8B) \end{cases}$$

Equation 7 is the solution that would be obtained if the two cells were perfectly coupled and behaved like a single supercell of length  $2L$ . Equations 8A and 8B are solutions for two isolated cells of length  $L$  each and are identical except for a coordinate shift of  $L$ . The  $V_m$  values for the two cells, each  $120 \mu\text{m}$  in length and stimulated with an  $E_o$  of  $10 \text{ V/cm}$ , are plotted in Figure 1A for three different coupling conditions: perfectly coupled cells ( $R_j = 0 \text{ M}\Omega$ ), cells with intermediate coupling ( $R_j = 50 \text{ M}\Omega$ ), and uncoupled cells ( $R_j \rightarrow \infty$ ). For these simulations  $r_i = 1.59 \times 10^8 \Omega/\text{cm}$  and  $r_m = 1.06 \times 10^6 \Omega\text{cm}$  were assumed.<sup>30</sup> STA was obtained as the difference in  $V_m$  for the two cells at  $x = 0$  and is given by Equation 9:

$$STA = \frac{4R_j E_o}{\kappa_s r_i} \sinh^2\left(\frac{L}{2\lambda}\right). \quad (9)$$

### Two Cells of Unequal Length

Similar to the equal cell length case, when  $R_j = 0$  Equations 3A and 3B reduce to Equation 10 (case of supercell), and when  $R_j \rightarrow \infty$ , they reduce to Equations 11A and 11B (case of separate isolated cells):

$$V_m = \frac{\lambda E_o}{\cosh\left(\frac{L1 + L2}{2\lambda}\right)} \sinh\left(\frac{x + \frac{L1 - L2}{2}}{\lambda}\right) \quad R_j = 0, \text{ all } x \quad (10)$$

$$V_m = \begin{cases} \frac{\lambda E_o}{\cosh(L1/2\lambda)} \sinh\left(\frac{x + \frac{L1}{2}}{\lambda}\right) & R_j \rightarrow \infty, x < 0 \quad (11A) \\ \frac{\lambda E_o}{\cosh(L2/2\lambda)} \sinh\left(\frac{x - \frac{L2}{2}}{\lambda}\right) & R_j \rightarrow \infty, x > 0. \quad (11B) \end{cases}$$

The  $V_m$  values for the two cells, with  $L1 = 150 \mu\text{m}$  and  $L2 = 90 \mu\text{m}$  (average length together of  $120 \mu\text{m}$ ) and stimulated with an  $E_o$  of  $10 \text{ V/cm}$ , are shown in Figure 1B for three different coupling conditions: perfectly coupled cells ( $R_j = 0 \text{ M}\Omega$ ), cells with intermediate coupling ( $R_j = 50 \text{ M}\Omega$ ), and two uncoupled cells ( $R_j \rightarrow \infty$ ). Note that at the junction between the two cells,  $V_m$  does not reverse polarity for the case of intermediate coupling. This outcome differs from that for the case of intermediate coupling between cells of equal length, in which  $V_m$  does change polarity at the junction (Fig. 1A). However, a reversal in  $V_m$  polarity for cells of unequal length can occur for certain values of  $R_j$ . These  $R_j$  values can be derived by substituting  $x = 0$  into Equations 3A and 3B so that we get:

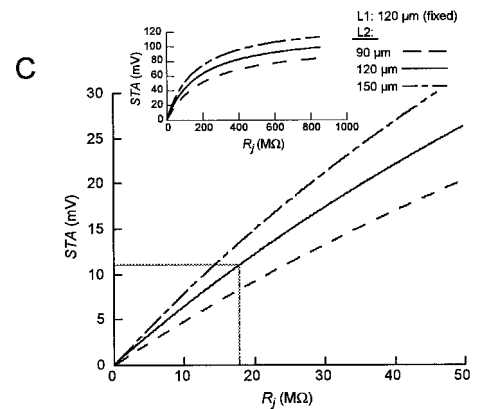
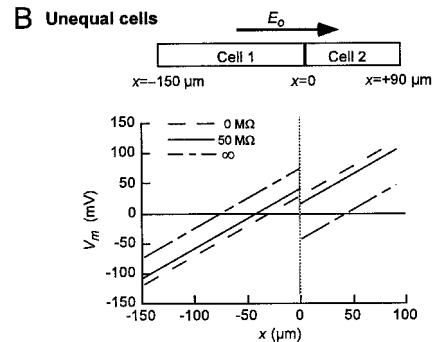
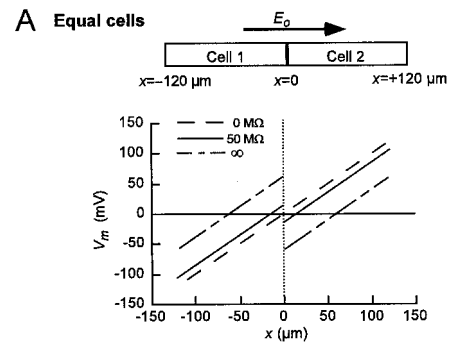


**Figure 1.** Theoretical transmembrane potential ( $V_m$ ) responses of two cells with variable coupling. (A) Steady-state  $V_m$  for two cells of equal length, stimulated longitudinally with a uniform electric field stimulus ( $E_o$ ) of  $10 \text{ V/cm}$ , for three different values of intercellular resistance ( $R_j$ ):  $0 \text{ M}\Omega$  (perfect coupling),  $50 \text{ M}\Omega$  (intermediate coupling), and completely uncoupled cells. Note that the sawtooth effect around the junction is accompanied by a reversal in the polarity of  $V_m$ . (B)  $V_m$  for two cells of unequal length, also for a field of  $10 \text{ V/cm}$  and three different values of  $R_j$  as in panel A. In this case, the sawtooth effect is not accompanied by a reversal in the polarity of  $V_m$  at the junction. (C) Sawtooth amplitude (STA) as a function of  $R_j$  for a cell-pair with constant  $L1$  of  $120 \mu\text{m}$ , and  $L2$  of  $90$ ,  $120$ , and  $150 \mu\text{m}$ . Inset shows the same plot over a wider range of  $R_j$ . As indicated by the wavy gray lines, an  $11\text{-mV}$  STA corresponds to an  $R_j$  of  $\sim 18 \text{ M}\Omega$ .

$$V_m = \begin{cases} \frac{2E_o}{\kappa} \left[ \alpha \sinh\left(\frac{L1 - L2}{2\lambda}\right) + \beta_1 \sinh\left(\frac{L1}{2\lambda}\right) \right] & x = 0^- \quad (12A) \\ \frac{2E_o}{\kappa} \left[ \alpha \sinh\left(\frac{L1 - L2}{2\lambda}\right) - \beta_2 \sinh\left(\frac{L2}{2\lambda}\right) \right] & x = 0^+. \quad (12B) \end{cases}$$

If  $L1 > L2$ , as is the case in Figure 1B,  $V_m$  in Equation 12A is always positive and, therefore,  $V_m$  in Equation 12B must be negative for a reversal in  $V_m$  to occur. Substituting

Equations 4A and 4C for  $\alpha$  and  $\beta_2$  into Equation 12B and solving for  $R_j$  for which  $V_m < 0$ , we get:

$$R_j > \frac{\lambda r_i \sinh\left(\frac{L1 + L2}{2\lambda}\right) \sinh\left(\frac{L1 - L2}{2\lambda}\right)}{\sinh\left(\frac{L1}{\lambda}\right) \sinh^2\left(\frac{L2}{2\lambda}\right)}. \quad (13)$$

Note that if  $L1 < L2$ , the form of Equation 13 remains the same, except that  $L1$  and  $L2$  are interchanged.

Thus, for a cell-pair with cells of different lengths, reversal in  $V_m$  polarity will occur at the junction only if  $R_j$  exceeds a critical value. It is interesting to note that because the right side of Equation 13 is independent of  $E_o$ , a change in  $E_o$  will change the slope of  $V_m$  and STA, but it will not cause a reversal in  $V_m$  when  $R_j$  remains less than the critical value. For the asymmetric cell-pair shown in Figure 1B, the critical value for  $R_j$  is  $\sim 136 \text{ M}\Omega$ . Note that the critical value is a function of the mismatch in the cell lengths and is zero for a symmetric cell-pair in which  $L1 = L2$ .

Finally, STA is given by:

$$STA = \frac{4R_j E_o}{\kappa r_i} \sinh\left(\frac{L1}{2\lambda}\right) \sinh\left(\frac{L2}{2\lambda}\right) \sinh\left(\frac{L1 + L2}{2\lambda}\right). \quad (14)$$

Figure 1C shows the variation of STA with  $R_j$  for  $E_o = 10 \text{ V/cm}$  applied to a cell-pair with  $L1$  fixed at  $120 \text{ }\mu\text{m}$ , and  $L2$  of  $90, 120,$  and  $150 \text{ }\mu\text{m}$ .

### Experimental Methods

Pairs of ventricular cells were enzymatically isolated from whole hearts of adult male guinea pigs (Hartley strain, weight 200 to 300 g) as follows. The animals were anesthetized with an intraperitoneal injection of sodium pentobarbital (0.1 mL/100 g; Abbott Labs, North Chicago, IL, USA) and injected with 0.1 to 0.3 mL of heparin to minimize clotting. Once the animal failed to respond to the paw pinch test, its chest was quickly opened via a radical medial thoracotomy. The heart was quickly excised, mounted on a Langendorff column, and perfused retrogradely through the aorta. Enzymatic dissociation was performed using the following sequence of solutions, all of which were oxygenated and maintained at  $37^\circ\text{C}$ : (1) 1.8 mM  $\text{Ca}^{2+}$  Tyrode's for 5 minutes; (2)  $\text{Ca}^{2+}$ -free Tyrode's for 7 minutes; (3) 50 mL  $\text{Ca}^{2+}$ -free Tyrode's with 0.25 mg/mL protease (type XIV; Sigma Chemical Co., St. Louis, MO, USA), 0.3 mg/mL collagenase (Worthington Biochemical Corp., Freehold, NJ, USA), and 1 mg/mL bovine serum albumin (type V; Sigma Chemical Co.) for 7 minutes; and (4)  $\text{Ca}^{2+}$ -free Tyrode for 5 minutes. After perfusion, the ventricles were chopped, gently stirred, and filtered to obtain isolated cells. During a few experimental sessions, the  $\text{Ca}^{2+}$  concentration during the intermediate  $\text{Ca}^{2+}$ -free phase of perfusion (step 2) was elevated to  $\sim 15 \text{ }\mu\text{M}$ . The elevated  $\text{Ca}^{2+}$  concentration has been shown to preserve intercellular gap junctions, thus helping to obtain cell-pairs with functionally intact gap junctions.<sup>31</sup> The yield of coupled cells usually was in the range of 1% to 2%.

The enzymatically isolated cell-pairs were stained with 25 to 50  $\mu\text{M}$  of the voltage-sensitive dye di-8-ANEPPS and loaded into a rotary experimental chamber that allowed the longitudinal axes of the cell-pairs to be aligned with field direction. The cells were stimulated using two (S1 and S2)

rectangular pulses with S1 and S2 durations of 5 and 10 msec, respectively, and an S1-S2 coupling interval of 20 msec. The S1 pulse elicited an action potential, and the S2 pulse was applied during the absolute refractory period. The fluorescence signals were recorded using a fiberoptic-based optical mapping system that was designed and built using an approach similar to that of Rohr and Kucera.<sup>32</sup> The dye-stained cells were excited using a 150-W short-arc xenon lamp (Opti Quip, Highland Mills, NY, USA), and the fluorescence signals were collected via a  $60\times$  (oil immersion, N.A. 1.3) or  $100\times$  (oil immersion, N.A. 1.3) objective. The fluorescence images of the specimen were projected onto an array of 149 optical fibers, each 1 mm in diameter. At  $60\times$  and  $100\times$  magnification, this resulted in a spatial resolution of 17 and 10  $\mu\text{m}$ , respectively. The signals from as many as 35 selected fibers were amplified and acquired into a computer at a sampling rate of 10 kHz per channel.

To discern the boundary of cell-pairs more clearly, fluorescent images of the cells stained with voltage-sensitive dye were taken. At the cell boundaries, the extensive membrane folding results in a higher dye density and consequently a higher intensity of the emitted fluorescence.

For all experiments, the S1 amplitude ( $<10 \text{ V/cm}$ ) was kept  $\sim 1$  to  $2 \text{ V/cm}$  above the excitation threshold, and the S2 amplitude ranged from 8 to 40 V/cm.  $V_m$  responses to the S2 pulse were used to estimate STA. To compare STA for cell-pairs with varying lengths, S2 amplitudes were scaled by  $(L1 + L2)/(2 \times 120)$ , where  $L1$  and  $L2$  represent the lengths (in  $\mu\text{m}$ ) of the two cells in the stimulated cell-pair. The scaled amplitude represents the equivalent electric field for a cell-pair with total length of  $240 \text{ }\mu\text{m}$ , twice the average length of  $120 \text{ }\mu\text{m}$  for a single guinea pig cardiac cell.<sup>28</sup>

We represent the transmembrane potential, which was recorded as a change in the emitted fluorescence, as  $V_m^F$ . The response to S2 ( $V_m^{F2}$ ) measured 0.75 msec after the make of the S2 pulse was obtained by normalizing the corresponding fluorescence change ( $\Delta F$ ) to the action potential amplitude ( $APA^F$ , refer to Fig. 3D, inset, for an example).  $V_m^{F2}$  was measured after a short delay of 0.75 msec from S2 onset to ensure that it consisted primarily of the passive response of the cell-pair.<sup>33</sup>

Statistical correlation between STA and S2 amplitude was determined by calculating Pearson's correlation coefficient  $R$  and conducting a two-tailed Student's  $t$ -test for rejecting the null hypothesis that the slope of the best fit line was zero and, therefore, that the parameters were not correlated.<sup>34</sup>  $P < 0.05$  was considered statistically significant.

### Experimental Results

Experiments were performed on a total of  $n = 14$  guinea pig ventricular cell-pairs with a total of 24 S1-S2 stimuli. To ensure that our recording system had the spatial resolution to detect polarization changes between two adjacent sites, control experiments were performed using pairs of adjacent but completely uncoupled cells. Figure 2 shows one such cell-pair that was stimulated with an S1-S2 pair ( $S1 = 8 \text{ V/cm}$ ,  $S2 = 33 \text{ V/cm}$ ) in the direction indicated by the arrow. A change in sign of  $V_m^{F2}$  is evident between the right-most site on cell 1 (bottom box) and left-most site on cell 2 (top box).

Figure 3A shows a guinea pig cell-pair ( $L1 = 109 \text{ }\mu\text{m}$ ,  $L2 = 125 \text{ }\mu\text{m}$ ) stimulated with an S1-S2 pulse pair ( $S1 =$

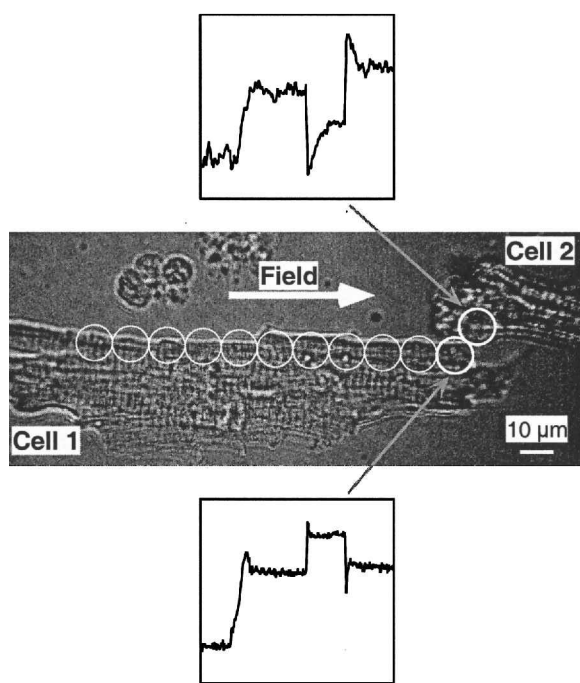


**Figure 2.** Control experiment showing large sawtooth amplitude for two completely uncoupled cells. The two cells were stimulated with a pair of S1-S2 pulses ( $S1 = 8$  V/cm,  $S2 = 33$  V/cm) in the direction indicated by the arrow.  $V_m^F$  signals recorded from two adjacent sites show a reversal in polarity, confirming the ability of the recording system to detect large polarization changes at a spatial resolution of  $10 \mu\text{m}$ . Original magnification  $\times 100$ .

6 V/cm,  $S2 = 20$  V/cm) in the direction indicated by the arrow. The intercellular junction (indicated by vertical arrow) is clearly delineated in the fluorescence image (Fig. 3B).  $V_m^F$  signals (Fig. 3C) were recorded from 23 sites (overlaid circles in Fig. 3A) and did not show any obvious reversal in polarization at the intercellular junction, giving an initial impression that no sawtooth was present. Figure 3D shows  $V_m^{F2}$  plotted along the length of the cell-pair by combining the data from the two rows. The data points have been staggered to match the geometry of the recording array. The straight lines were drawn through the data points for the two cells within the theoretical constraint that the slope of two lines be equal and were found to have an excellent fit ( $R > 0.99$  for both cells). The discontinuity in the linear fits at the intercellular junction was used to estimate STA. For the cell-pair shown in Figure 3, STA was estimated to be  $\sim 27$  mV (calculated assuming  $APA^F$  of  $\sim 128$  mV for a typical guinea pig cardiac cell<sup>28</sup>). From Equation 14, the corresponding  $R_j$  was estimated to be  $23 \text{ M}\Omega$ , which is less than the critical  $R_j$  of  $\sim 27 \text{ M}\Omega$  (computed using Equation 13) required for polarity reversal across the junction. Thus, the observed discontinuity in  $V_m^F$  response that is superimposed on a depolarizing offset (Fig. 3D) is consistent with the theory, despite a slight hyperpolarizing trend in the responses during the S2 pulse (Fig. 3C).

To confirm that the slope discontinuities were indeed the result of intercellular gap junctions, we performed a few experiments ( $n = 3$ ) in which the cell-pairs were exposed to 2.5 mM heptanol, a potent gap junction uncoupler.<sup>35</sup> A typical result from such an experiment is shown in Figure 4.

Figures 4A and 4B show the bright-field and fluorescence images of a cell-pair, respectively ( $L1 = 113 \mu\text{m}$ ,  $L2 = 121 \mu\text{m}$ ).  $V_m^F$  recordings for the cell-pair were obtained in response to three successive S1-S2 pulse pairs ( $S1 = 5$  V/cm,  $S2 = 22$  V/cm) separated by approximately 10-minute intervals for control, heptanol, and washout conditions. Although the responses varied monotonically along the length of the cell-pair for control and washout conditions, a reversal in response polarity across the intercellular junction was observed for heptanol (Fig. 4C). From  $V_m^{F2}$  plotted along the length of the cell-pair, STA was estimated to be  $\sim 23$  mV for the control condition. The STA increased 10-fold to  $\sim 256$  mV upon exposure to heptanol and decreased to  $\sim 33$  mV upon drug washout. The STA for heptanol was found to be approximately equal to the theoretically expected value of 257 mV for completely uncoupled cells. Note that an action potential was not elicited for heptanol and washout conditions; therefore, action potential amplitude was not available to normalize these traces. Exploiting the fact that the baseline fluorescence levels for the three conditions were approximately equal, we used raw  $APA^F$  of the control recordings from the various sites to scale the heptanol and

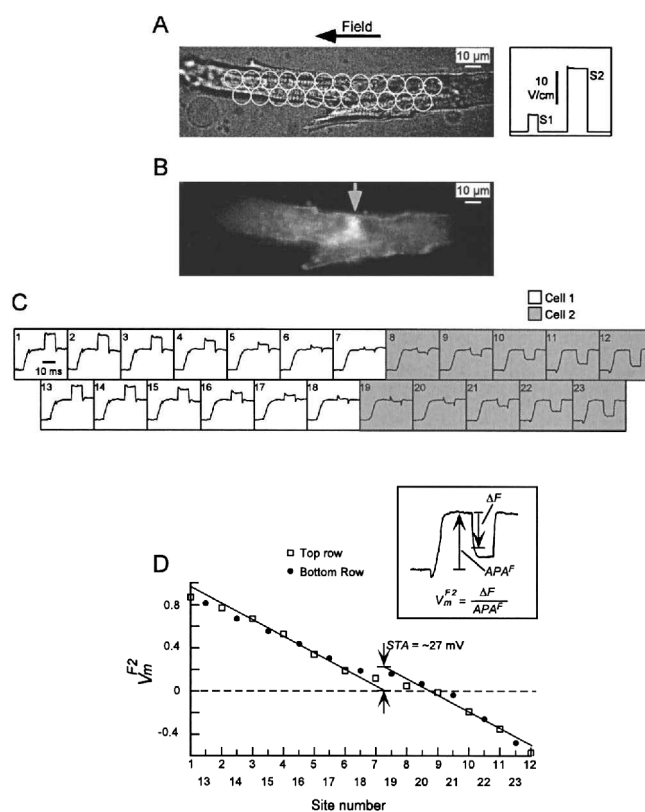


**Figure 3.**  $V_m^F$  signals recorded from a cell-pair and estimation of sawtooth amplitude (STA). (A) Cell-pair that was stimulated with an S1-S2 pair ( $S1 = 6$  V/cm,  $S2 = 20$  V/cm) shown alongside the cell and in the direction indicated by the arrow. (B) Fluorescence picture of the cell-pair in which the intercellular junction is clearly delineated as a brightly lit region. (C) Boxes numbered 1 through 23 show  $V_m^F$  signals recorded from the cell-pair corresponding to the two rows of sites on the cell-pair. From the recordings, a large sawtooth is not readily apparent. (D) Response to the S2 pulse ( $V_m^{F2}$ ) along the length of the cell-pair by merging the data of the two rows of sites.  $V_m^{F2}$  is linear over the extent of each individual cell (fitted lines) but shows a discontinuity near the junction that is equal to STA. Original magnification  $\times 100$ .

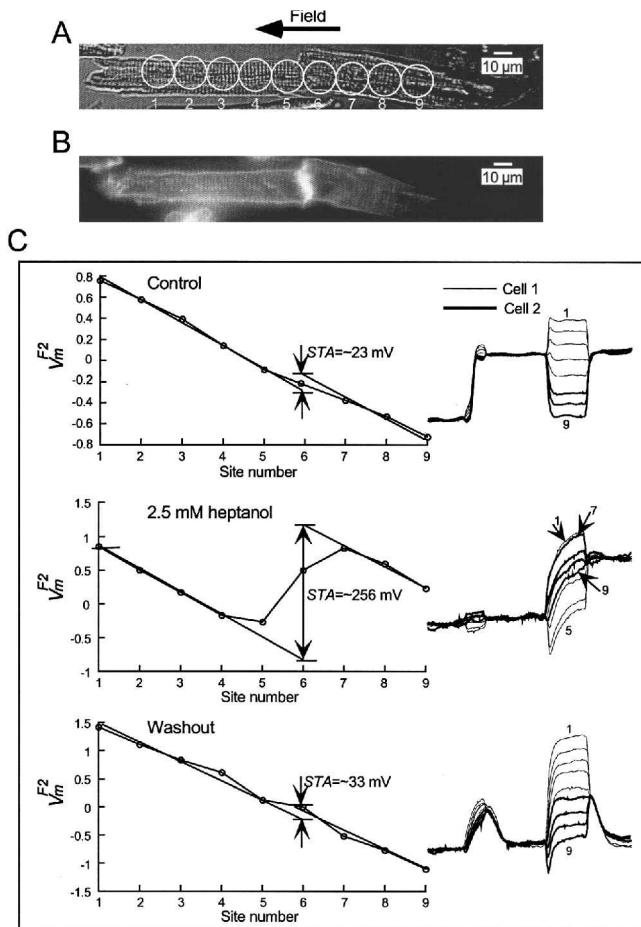


**Figure 4.** Augmentation of sawtooth amplitude (STA) upon exposure to heptanol. (A,B) Bright-field and fluorescence pictures of a cell-pair that was stimulated with successive S1-S2 pulse pairs (S1 = 5 V/cm, S2 = 22 V/cm), and  $V_m^F$  recorded under control, 2.5 mM heptanol, and washout conditions. The interval between the pulse pairs was ~ 10 minutes. (C)  $V_m^{F2}$  along the cell length and  $V_m^F$  signals superimposed from the nine sites for the three conditions. STA was ~ 23 mV for control condition, increased to ~ 256 mV for heptanol, and decreased to ~ 33 mV upon heptanol washout. Original magnification  $\times 60$ .

washout recordings for the corresponding sites, e.g.,  $APA^F$  of control recording from site 1 was used to scale heptanol and washout recordings from site 1.

The discontinuities in  $V_m^{F2}$ , similar to those shown in Figures 3D and 4C, were observed in 12 other cell-pairs in addition to those shown in Figures 3 and 4. The results from all 14 cell-pairs and 24 S1-S2 stimuli are summarized in Figure 5. STA increased monotonically with S2 amplitude, having a slope of 1.3 mV/V/cm ( $R = 0.77$ ,  $P < 0.001$ ). STA values were scaled by a factor of  $10/(S2 \text{ amplitude})$  to determine the mean STA for a nominal 10 V/cm field and was found to be  $11 \pm 4$  mV. From the theoretically derived relationship between STA and  $R_j$  for a symmetric cell-pair (Fig. 1C), an 11-mV STA corresponds to an  $R_j$  of 17.9  $M\Omega$ , which is well within the physiologic range.

### Discussion

In this study, we present a theoretical relationship between STA and junctional resistance  $R_j$ , and experimental measurements of STA in coupled guinea pig ventricular

cell-pairs obtained by optical maps of field responses at a high (subcellular) resolution. The major results of our study are as follows. (1) Theoretically, we show that the transmembrane voltage  $V_m$  is expected to vary linearly along the length of each individual cell in a cell-pair, and the sawtooth effect should manifest as a discontinuity in  $V_m$  at the intercellular junction. (2) For an asymmetric cell-pair (i.e., cell-pair with two cells of unequal lengths), the sawtooth effect can manifest without a reversal in  $V_m$  polarity, provided  $R_j$  is less than a critical value. The critical  $R_j$  depends on the lengths of the two cells constituting the cell-pair (Equation 13). (3) Experimentally recorded optical  $V_m$  responses from discrete sites on a cell can be fit with straight lines for each cell in a cell-pair. When the straight lines are extrapolated to the intercellular junction, a discontinuity is observed that can be used to determine STA. (4) Consistent with our theoretical analysis, the sawtooth effect is observed without a  $V_m$  polarity reversal when the estimated  $R_j$  value is less than the critical  $R_j$  (Figs. 3C and 3D). (5) When the intercellular junction is uncoupled by exposure to heptanol, STA increases to the theoretically expected value for two adjacent isolated cells (Fig. 4C). (6) Based on experiments with 14 cell-pairs, we estimate STA to be ~ 11 mV for a nominal 10 V/cm field (Fig. 5), which corresponds to a calculated  $R_j$  of ~ 18  $M\Omega$ .

Some differences were observed between theory and experiment. In contrast to our theoretical results in which an abrupt change in  $V_m$  occurs at the intercellular junction (Figs. 1A and 1B), the experimental data show a smoother transition in  $V_m$  (Figs. 3D and 4C). Because cardiac cells are ~ 5 to 20  $\mu\text{m}$  thick<sup>23,25</sup> and the fluorescence recordings usually are obtained by having 1 of the 2 cell surfaces in focus, the signal from the out-of-focus surface is smeared and could be a source of cross-talk among signals from adjacent sites. Even upon exposure to heptanol, which presumably uncoupled the cells completely, the transition in  $V_m$  across the junction remained smooth and hence supports this conjecture.

From our theoretical results, it is clear that reversal in  $V_m$  polarity occurs at the intercellular junction only under certain conditions and is an overly stringent definition of the

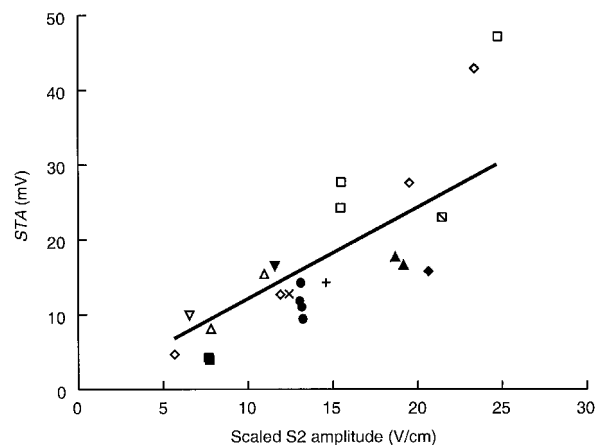


**Figure 5.** Results from all cell-pairs. The sawtooth amplitude (STA) similar to that shown in Figures 3D and 4C was estimated in 12 other cell-pairs and the results are summarized. STA increased monotonically with the S2 amplitude with a slope of 1.3 mV/V/cm ( $R = 0.77$ ,  $P < 0.001$ ).

sawtooth effect. In general, the sawtooth pattern of polarization can be superimposed on a depolarizing or hyperpolarizing level of  $V_m$ . The offset arises when the intercellular junction is closer to one edge of the cell-pair, as is the case for a pair with cells of unequal lengths, so that the effects of opposing (depolarizing and hyperpolarizing) secondary sources from the two edges do not cancel (Fig. 1B). In tissue, a similar scenario can arise if the region of observation is located closer to one tissue surface versus another, resulting in global hyperpolarization or depolarization of the region. In such cases, the sawtooth effect will be manifested as a reversal in  $V_m$  polarity only if the cells are highly uncoupled and  $R_j$  is very high. To better understand this situation, consider the commonly treated case of a linear strand of cells that is several space constants in length. The sawtooth is superimposed over a nonoscillatory offset potential that varies monotonically from hyperpolarization at the anodal end to depolarization at the cathodal end.<sup>10,36</sup> Therefore, under normal coupling conditions, only the cells in the middle of the strand will show a reversal in  $V_m$  at the intercellular junction. As  $R_j$  is increased, the offset potential will decrease with a simultaneous increase in STA so that now the cells closer to an edge (within a space constant) also may show a reversal in  $V_m$  polarity. In the extreme case when the cells are completely uncoupled ( $R_j \rightarrow \infty$ ), every cell in the strand behaves as an isolated cell; therefore, even the cells at the strand ends will show a reversal in  $V_m$  polarity.

Defining the sawtooth effect strictly as a reversal in  $V_m$  polarity may explain why some of the previous studies failed to reveal a clear-cut sawtooth effect in multicellular structures.<sup>21,22</sup> A closer examination of data of Zhou et al.<sup>22</sup> recorded from papillary muscle reveals undulations in  $V_m$  (approximately on the length scale of a cell) riding on a global depolarizing or hyperpolarizing response along the length of their papillary muscle. It is conceivable that some of these undulations were the result of a spatially averaged sawtooth. A global depolarizing or hyperpolarizing response also was present in the recordings of Gillis et al.<sup>21</sup> obtained from cultured monolayers, making it possible that the sawtooth effect was obscured. However, in their case, no significant difference was found in the transmembrane potential gradient across the intercellular junction compared with that over the cell length, arguing against the presence of a sawtooth effect. The reasons for this finding may be several. First, as mentioned by Gillis et al.,<sup>21</sup> the cells in cultured monolayers have gap junctions uniformly distributed around the cell edges, in contrast to adult tissue where the gap junctions are located primarily at the longitudinal ends. This can depress, but not eliminate, STA via lateral electrotonic interactions, as suggested by several modeling studies.<sup>13,14</sup> Second, the cultured neonatal cardiac rat cells are  $\sim 50$  to  $70 \mu\text{m}$  long<sup>37</sup> and, therefore, are significantly shorter than adult ventricular cells (e.g., guinea pig cells typically are  $120 \mu\text{m}$  long<sup>28</sup>). Because STA is a strong function of cell length (Equations 9 and 14), STA in cultured cells would be smaller for a given field intensity. Third, some signal averaging in the fluorescence measurements can arise because of the finite thickness of the cells, as mentioned earlier. These three factors may explain the failure by Gillis et al.<sup>21</sup> to observe any significant change in transmembrane potential gradients across the intercellular junctions. However, in light of the fact that the reported  $R_j$

is  $\sim 30 \text{ M}\Omega$  in cultured cells,<sup>38</sup> a complete abolishment of the sawtooth effect is unexpected given our theoretical analysis and that of other modeling studies.<sup>13,14</sup>

In a linear strand that is several space constants long, STA in the middle of the strand is expected to be larger than at the ends.<sup>10,36</sup> This is because the extracellular current produced by the external field redistributes partially into the cells and reaches equilibrium in regions more than a space constant away from the strand ends. Therefore, in the middle of the strand, the intracellular axial current is maximal, resulting in the largest voltage drop across the junction and producing the largest STA. Because the length of a cell-pair ( $\sim 240 \mu\text{m}$ ) is significantly smaller than the space constant ( $\sim 1 \text{ mm}$ ), STA of  $\sim 11 \text{ mV}$  per  $10 \text{ V/cm}$  in cell-pairs is expected to be lower than that in a strand of cells in regions far from its ends, given that extracellular current has not had enough distance to equilibrate across membranes of the cell-pair. On the other hand, in tissue, which can be considered roughly as an assembly of many such strands in parallel, STA will be depressed owing to electrotonic interactions among cells (*lateral averaging*) and will depend on the number of lateral interconnections.<sup>13,14</sup> The aforementioned modeling studies<sup>13,14</sup> predict that STA in regions of the myocardium farther than a space constant from the tissue surfaces can be much larger than our STA estimate in isolated cell-pairs (e.g., Juhlin and Pormann<sup>14</sup> predict an STA of  $25.2 \text{ mV}$  per  $10 \text{ V/cm}$  for the most severe case of interstrand electrotonic interaction). This might imply that the STA-accentuating effect of increasing intracellular current can compensate for the STA-diminishing effect of lateral averaging in the bulk of the myocardium. Unfortunately, the lack of good experimental techniques to measure transmembrane potential from the depths of the myocardium makes direct verification of a sawtooth effect in tissue a challenge. Perhaps future improvements in spatial and temporal resolution of the confocal-type or two-photon-type microscopy might pave the way for a solution to this difficult problem.

Numerous studies are available on  $R_j$  measurements in multicellular structures (tissue and cultured monolayers). The estimates of  $R_j$  vary widely and range from  $\sim 1 \text{ M}\Omega$ <sup>24</sup> to tens of megaohms.<sup>38,39</sup> Some of the uncertainty arises because of the numerous assumptions that must be made in deducing  $R_j$ , e.g., structural details (monodomain, bidomain, etc.) of the underlying structure.<sup>40</sup> Isolated cell-pairs have been widely used as a simplified system to measure  $R_j$ . However, they too have yielded a wide range of  $R_j$  values. Weingart and Maurer<sup>26</sup> reported  $R_j$  ranging from  $5 \text{ M}\Omega$  to  $>780 \text{ M}\Omega$  in guinea pig and rat cell-pairs. They found that for  $R_j$  in the range from  $5$  to  $265 \text{ M}\Omega$ , the cells were normally coupled, evident from negligible conduction delay across the junction. In the range from  $155$  to  $375 \text{ M}\Omega$ , conduction delays were detectable, and for  $R_j > 780 \text{ M}\Omega$ , complete conduction block occurred. White et al.<sup>25</sup> reported  $R_j$  to be  $\sim 101 \text{ M}\Omega$  in adult rat myocytes. Daleau<sup>41</sup> reported a mean value of  $24 \text{ M}\Omega$  for isolated guinea pig ventricular cell-pairs. Verheule et al.<sup>42</sup> reported a mean value of  $\sim 6 \text{ M}\Omega$  for isolated rabbit ventricular cell-pairs. However, Kieval et al.<sup>27</sup> reported a much lower mean value of  $\sim 1 \text{ M}\Omega$  in rabbit cell-pairs. Wittenberg et al.<sup>31</sup> reported an even lower value of  $\sim 0.4 \text{ M}\Omega$  in adult rat myocyte-pairs. Based on our theoretical relationship between STA and  $R_j$ , these reported values of  $R_j$  would span an STA range of  $\sim 1$  to

~ 70 mV for a nominal 10 V/cm field (Fig. 1C). Our experimental measurements of STA suggest an  $R_j$  value of ~ 18 M $\Omega$ , which is well within the range of normal coupling resistances in isolated cell-pairs noted earlier.<sup>25,26</sup>

Similar to some of the other cell-pair studies, our  $R_j$  estimate is higher than the value that can be computed indirectly from reported intracellular conductance values of intact tissue.<sup>24,43,44</sup> As we alluded to earlier, one possible reason for this is that models used to derive  $R_j$  from tissue level measurements do not capture the structural complexity of cardiac tissue and, therefore, may be inaccurate. Another possibility is that isolated cell-pairs do not reflect true intercellular resistance of intact tissue because it is modified during the cell isolation procedure. Unfortunately, to date no experimental study exists that directly compares  $R_j$  in isolated cell-pairs to  $R_j$  in intact tissue.

Although we focused primarily on STA in longitudinally coupled cell-pairs, we also examined a few ( $n = 2$ ) transversely coupled cell-pairs. Because a typical cell-pair is only ~ 20 to 30  $\mu\text{m}$  wide, we were able to record responses from only 2 to 3 detectors (at 100 $\times$  magnification) along the cell width; therefore, our experimental approach used to estimate STA in longitudinally coupled cell-pairs could not be applied. However, in these cell-pairs, a large sawtooth effect, as would be accompanied by  $V_m$  polarity reversal across the junction, was not observed. We might not expect to observe a significant transverse STA for two reasons. First, the cell dimension in the transverse direction is smaller than in the longitudinal direction, so that STA would be smaller for a given field intensity. Second, the flow of intracellular current will be smaller in the transverse direction compared with the longitudinal direction, due to the higher transverse intracellular resistance that results from the shorter cell width and the lower density of lateral gap junctions (in adult myocardium). Thus, the transverse STA will be augmented to a lesser degree by intracellular current flow compared with the longitudinal STA.

### Implications

A number of modeling studies suggest that the sawtooth effect might be an important component of the elusive “missing link” between the external electric field and resulting tissue polarization.<sup>12,13,15,45-47</sup> For example, Fishler et al.<sup>12</sup> showed that in a strand of cardiac cells modeled with Luo-Rudy phase I membrane kinetics,<sup>48</sup> an approximately 40-mV STA in response to a shock applied at the wave tail of a previously propagating wavefront produced a graded depolarization along the length of the strand and resulted in a new propagating wavefront. In the absence of any sawtooth effect, the shock was incapable of modifying the previous wavefront. In another recent modeling study, Wall et al.<sup>47</sup> replicated the experiment of Frazier et al.<sup>49</sup> in a 2-D sheet of cardiac tissue with equal anisotropy. They showed that with sawtooth effect included (with STA proportional to the external field amplitude and cell length), cross-field stimulation could produce critical points and reentrant activity in their 2-D sheet tissue model, much like the experimental reentry of Frazier et al. Considering that their electric field was set to match the experimental conditions of Frazier et al., STA of up to ~ 60 mV could be present at the site of the critical point. We estimate an average STA of ~ 11 mV for a 10 V/cm field in isolated cell-pairs. However,

as we discussed earlier, STA measured in isolated cell-pairs could underestimate STA in tissue for comparable field strengths. Another possibility is that because no single mechanism seems to fully account for polarization large enough required to explain experimentally observed phenomena (such as critical point and reentry),<sup>50</sup> it is possible that the synergistic effect of multiple mechanisms, such as sawtooth effect and polarization via fiber direction and branching, might be a key to understanding the “missing link” alluded to earlier.

As an extrapolation of our isolated cell-pair results to tissue, we speculate that even a smaller STA that induces subthreshold level depolarization has the potential to modify tissue response. The reason for this rests in the nonlinear properties of the cardiac cell membranes that can cause a net current to flow across the cell membrane during field stimulation, and depolarize or hyperpolarize the cells. The polarity of the current and the ion channels involved in these field-induced changes in transmembrane currents vary with the phase of the action potential. For example, a shock applied during rest causes a net inward current and depolarizes the tissue. Modeling studies have implicated a net inward current via sodium channels and inwardly rectifying potassium channels as the basis of this depolarization.<sup>51,52</sup> In contrast to depolarization at rest, a shock applied during the absolute refractory phase results in net outward current and tissue hyperpolarization. An imbalance in L-type calcium currents has been attributed as a cause of such hyperpolarization responses in strands of cultured neonatal rat cardiac myocytes.<sup>53</sup> Thus, the presence of a sawtooth effect implies that depolarizing or hyperpolarizing responses would occur in tissue that otherwise would have remained unaffected by the shock. For a given  $R_j$ , the amount of depolarization or hyperpolarization will depend on the shock strength and pulse parameters (e.g., shape and duration). It is conceivable that these polarizations can interact with existing wavefronts and modify their spatial and temporal evolution.

During pathophysiologic conditions, such as ischemia, cells undergo an increase in intracellular pH, which causes closure of gap-junction-forming connexin43 channels<sup>54</sup> and heterogeneous loss of connexin43.<sup>55</sup> Both of these actions will result in cellular uncoupling and increase  $R_j$ . Furthermore, severe ischemia can cause myocardial infarction. At the border zone of the infarcted region, the longitudinal cell-to-cell gap junctions disappear right after infarction. Thereafter, they undergo abnormal remodeling as the tissue heals and become extensively distributed over the lateral borders of the cells.<sup>56,57</sup> Consequently,  $R_j$  is expected to be relatively high in the infarct border zone, and the potential role of the sawtooth effect under such conditions may become even more prominent in determining the outcome of a defibrillation shock.

### Appendix

We solve Equation 1 for cell 1 ( $x < 0$ ) and cell 2 ( $x > 0$ ) separately and then couple the two solutions at the intercellular junction using the boundary conditions for  $I_i$  (refer to Theoretical section). The most general solutions of Equation 1 for the two cells are:

$$V_m = Ae^{x/\lambda} + Be^{-x/\lambda} \quad x < 0 \quad (\text{A-1A})$$

$$V_m = Ce^{x/\lambda} + De^{-x/\lambda} \quad x > 0. \quad (\text{A-1B})$$

Applying the sealed end boundary conditions to the above equations:

$$Ae^{-L_1/\lambda} - Be^{L_1/\lambda} = \lambda E_o \quad (\text{A-2A})$$

$$Ce^{L_2/\lambda} - De^{-L_2/\lambda} = \lambda E_o. \quad (\text{A-2B})$$

The continuity of  $I_i$  at the intercellular junction leads to:

$$A - B = C - D. \quad (\text{A-2C})$$

And finally, application of Kirchhoff's voltage law at the junction yields:

$$(A + B) - (C + D) = \frac{-R_j}{\lambda r_i} (A - B) + \frac{E_o R_j}{r_i}. \quad (\text{A-2D})$$

Equations A-2A to A-2D constitute four independent equations in four variables and can be easily solved to obtain  $A$ ,  $B$ ,  $C$ , and  $D$ . The equations yield:

$$A = \frac{E_o(\alpha e^{(L_1-L_2)/2\lambda} + \beta_1 e^{L_1/2\lambda})}{\lambda} \quad (\text{A-3A})$$

$$B = -\frac{E_o(\alpha e^{-(L_1-L_2)/2\lambda} + \beta_1 e^{-L_1/2\lambda})}{\kappa} \quad (\text{A-3B})$$

$$C = \frac{E_o(\alpha e^{(L_1-L_2)/2\lambda} + \beta_2 e^{L_1/2\lambda})}{\kappa} \quad (\text{A-3C})$$

$$D = -\frac{E_o(\alpha e^{-(L_1-L_2)/2\lambda} + \beta_2 e^{-L_1/2\lambda})}{\kappa} \quad (\text{A-3D})$$

where  $\alpha$ ,  $\beta_1$ ,  $\beta_2$ , and  $\kappa$  are as given in Equations 4A to 4D.

Substituting for the constants in Equations A-1A and A-1B and simplifying, we obtain  $V_m$  as given by Equations 3A and 3B.

## References

- Colavita PG, Wolf P, Smith WM, Bartram FR, Hardage M, Ideker RE: Determination of effects of internal countershock by direct cardiac recordings during normal rhythm. *Am J Physiol* 1986;250:H736-H740.
- Kwaku KF, Dillon SM: Shock-induced depolarization of refractory myocardium prevents wave-front propagation in defibrillation. *Circ Res* 1996;79:957-973.
- Witkowski FX, Kerber RE: Currently known mechanisms underlying direct current external and internal cardiac defibrillation. *J Cardiovasc Electrophysiol* 1991;2:562-572.
- Trayanova N, Skouibine K, Aguel F: The role of cardiac tissue structure in defibrillation. *Chaos* 1998;8:221-233.
- Trayanova NA, Roth BJ, Malden LJ: The response of a spherical heart to a uniform electric field: A bidomain analysis of cardiac stimulation. *IEEE Trans Biomed Eng* 1993;40:899-908.
- Sobie EA, Susil RC, Tung L: A generalized activating function for predicting virtual electrodes in cardiac tissue. *Biophys J* 1997;73:1410-1423.
- Entcheva E: Influence of the electric axis of stimulation on the induced transmembrane potentials in ellipsoidal bidomain heart. *Ann Biomed Eng* 2000;28:244-252.
- Fast VG, Rohr S, Gillis AM, Kleber AG: Activation of cardiac tissue by extracellular electrical shocks: Formation of "secondary sources" at intercellular clefts in monolayers of cultured myocytes. *Circ Res* 1998;82:375-385.
- Fishler MG: Syncytial heterogeneity as a mechanism underlying cardiac far-field stimulation during defibrillation-level shocks. *J Cardiovasc Electrophysiol* 1998;9:384-394.
- Plonsey R, Barr RC: Inclusion of junction elements in a linear cardiac model through secondary sources: Application to defibrillation. *Med Biol Eng Comput* 1986;24:137-144.
- Cartee LA, Plonsey R: The effect of cellular discontinuities on the transient subthreshold response of a one-dimensional cardiac model. *IEEE Trans Biomed Eng* 1992;39:260-270.
- Fishler MG, Sobie EA, Tung L, Thakor NV: Modeling the interaction between propagating cardiac waves and monophasic and biphasic field stimuli: The importance of the induced spatial excitatory response. *J Cardiovasc Electrophysiol* 1996;7:1183-1196.
- Krinsky V, Pumir A: Models of defibrillation of cardiac tissue. *Chaos* 1998;8:188-203.
- Juhlin SP, Pormann JB: Dimensional comparison of the sawtooth pattern in transmembrane potential. *Comput Cardiol* 1994:413-416.
- Trayanova N: Discrete versus syncytial tissue behavior in a model of cardiac stimulation—I: Mathematical formulation. *IEEE Trans Biomed Eng* 1996;43:1129-1140.
- Krassowska W, Frazier DW, Pilkington TC, Ideker RE: Potential distribution in three-dimensional periodic myocardium—Part II: Application to extracellular stimulation. *IEEE Trans Biomed Eng* 1990;37:267-284.
- Knisley SB, Blitchington TF, Hill BC, Grant AO, Smith WM, Pilkington TC, Ideker RE: Optical measurements of transmembrane potential changes during electric field stimulation of ventricular cells. *Circ Res* 1993;72:255-270.
- Windisch H, Ahammer H, Schaffer P, Muller W, Platzer D: Optical multisite monitoring of cell excitation phenomena in isolated cardiomyocytes. *Pflugers Arch* 1995;430:508-518.
- Cheng DKL, Tung L, Sobie EA: Nonuniform responses of transmembrane potential during electric field stimulation of single cardiac cells. *Am J Physiol* 1999;277(Heart Circ Physiol 46):H351-H362.
- Sharma V, Tung L: Transmembrane responses of single guinea pig myocyte to uniform electric field stimulus. *J Cardiovasc Electrophysiol* 1999;10:1296.
- Gillis AM, Fast VG, Rohr S, Kleber AG: Spatial changes in transmembrane potential during extracellular electrical shocks in cultured monolayers of neonatal rat ventricular myocytes. *Circ Res* 1996;79:676-690.
- Zhou X, Knisley SB, Smith WM, Rollins D, Pollard AE, Ideker RE: Spatial changes in the transmembrane potential during extracellular electric stimulation. *Circ Res* 1998;83:1003-1014.
- Sommer JR, Scherer B: Geometry of cell and bundle appositions in cardiac muscle: Light microscopy. *Am J Physiol* 1985;248:H792-H803.
- Chapman RA, Fry CH: An analysis of the cable properties of frog ventricular myocardium. *J Physiol (Lond)* 1978;283:263-282.
- White RL, Spray DC, Campos de Carvalho AC, Wittenberg BA, Bennett MV: Some electrical and pharmacological properties of gap junctions between adult ventricular myocytes. *Am J Physiol* 1985;249:C447-C455.
- Weingart R, Maurer P: Action potential transfer in cell pairs isolated from adult rat and guinea pig ventricles. *Circ Res* 1988;63:72-80.
- Kieval RS, Spear JF, Moore EN: Gap junctional conductance in ventricular myocyte pairs isolated from postischemic rabbit myocardium. *Circ Res* 1992;71:127-136.
- Watanabe T, Rautaharju PM, McDonald TF: Ventricular action potentials, ventricular extracellular potentials, and the ECG of guinea pig. *Circ Res* 1985;57:362-373.
- Weidmann S: Electrical constants of trabecular muscle from mammalian heart. *J Physiol (Lond)* 1970;210:1041-1054.
- Plonsey R, Barr RC: Effect of microscopic and macroscopic discontinuities on the response of cardiac tissue to defibrillating (stimulating) currents. *Med Biol Eng Comput* 1986;24:130-136.
- Wittenberg BA, White RL, Ginzberg RD, Spray DC: Effect of calcium on the dissociation of the mature rat heart into individual and paired myocytes: Electrical properties of cell pairs. *Circ Res* 1986;59:143-150.
- Rohr S, Kucera JP: Optical recording system based on a fiber optic image conduit: Assessment of microscopic activation patterns in cardiac tissue. *Biophys J* 1998;75:1062-1075.
- Sharma V, Tung L: Analysis of field-induced transmembrane potential responses of single cardiac cells in terms of active and passive components. In: *World Congress on Medical Physics and Biomedical Engineering*. Chicago, Illinois, 2000, Abstract WE-E327-04.
- Pagano M, Gauvreau K: *Principles of Biostatistics*. Duxbury Press, Belmont, CA, 1993.
- Bastiaanse EM, Jongsma HJ, van der Laarse A, Takens-Kwak BR:

- Heptanol-induced decrease in cardiac gap junctional conductance is mediated by a decrease in the fluidity of membranous cholesterol-rich domains. *J Membr Biol* 1993;136:135-145.
36. Trayanova N, Pilkington TC: A bidomain model with periodic intracellular junctions: A one-dimensional analysis. *IEEE Trans Biomed Eng* 1993;40:424-433.
  37. Rohr S, Scholly DM, Kleber AG: Patterned growth of neonatal rat heart cells in culture. Morphological and electrophysiological characterization. *Circ Res* 1991;68:114-130.
  38. Fluri GS, Rudisuli A, Willi M, Rohr S, Weingart R: Effects of arachidonic acid on the gap junctions of neonatal rat heart cells. *Pflugers Arch* 1990;417:149-156.
  39. Fast VG, Kleber AG: Microscopic conduction in cultured strands of neonatal rat heart cells measured with voltage-sensitive dyes. *Circ Res* 1993;73:914-925.
  40. Plonsey R, Barr RC: A critique of impedance measurements in cardiac tissue. *Ann Biomed Eng* 1986;14:307-322.
  41. Daleau P: Effects of antiarrhythmic agents on junctional resistance of guinea pig ventricular cell pairs. *J Pharmacol Exp Ther* 1998;284:1174-1179.
  42. Verheule S, van Kempen MJ, te Welscher PH, Kwak BR, Jongsma HJ: Characterization of gap junction channels in adult rabbit atrial and ventricular myocardium. *Circ Res* 1997;80:673-681.
  43. Clerc L: Directional differences of impulse spread in trabecular muscle from mammalian heart. *J Physiol* 1976;255:335-346.
  44. Roberts DE, Scher AM: Effect of tissue anisotropy on extracellular potential fields in canine myocardium in situ. *Circ Res* 1982;50:342-351.
  45. Krassowska W, Pilkington TC, Ideker RE: Periodic conductivity as a mechanism for cardiac stimulation and defibrillation [published erratum appears in *IEEE Trans Biomed Eng* 1987;34:835]. *IEEE Trans Biomed Eng* 1987;34:555-560.
  46. Keener JM: The effect of gap junctional distribution on defibrillation. *Chaos* 1998;8:175-187.
  47. Wall J, Trayanova N, Skouibine K, Krassowska W: Modeling induction of reentry with realistic S2 stimulus. In: *The First Joint BMES/EMBS Conference, Atlanta, Georgia, 1999*:154.
  48. Luo CH, Rudy Y: A model of the ventricular cardiac action potential. Depolarization, repolarization, and their interaction. *Circ Res* 1991;68:1501-1526.
  49. Frazier DW, Wolf PD, Wharton JM, Tang AS, Smith WM, Ideker RE: Stimulus-induced critical point. Mechanism for electrical initiation of reentry in normal canine myocardium. *J Clin Invest* 1989;83:1039-1052.
  50. Roth BJ, Krassowska W: The induction of reentry in cardiac tissue. The missing link: How electric fields alter transmembrane potential. *Chaos* 1998;8:204-220.
  51. Tung L, Borderies JR: Analysis of electric field stimulation of single cardiac muscle cells. *Biophys J* 1992;63:371-386.
  52. Krassowska W, Neu JC: Response of a single cell to an external electric field. *Biophys J* 1994;66:1768-1776.
  53. Cheek ER, Ideker RE, Fast VG: Nonlinear changes of transmembrane potential during defibrillation shocks: Role of  $Ca^{2+}$  current. *Circ Res* 2000;87:453-459.
  54. Morley GE, Ek-Vitorin JF, Taffet SM, Delmar M: Structure of connexin43 and its regulation by pH. *J Cardiovasc Electrophysiol* 1997;8:939-951.
  55. Huang X, Sandusky GE, Zipes DP: Heterogeneous loss of connexin43 protein in ischemic dog hearts. *J Cardiovasc Electrophysiol* 1999;10:79-91.
  56. Smith JH, Green CR, Peters NS, Rothery S, Severs NJ: Altered patterns of gap junction distribution in ischemic heart disease. An immunohistochemical study of human myocardium using laser scanning confocal microscopy. *Am J Pathol* 1991;139:801-821.
  57. Matsushita T, Oyamada M, Fujimoto K, Yasuda Y, Masuda S, Wada Y, Oka T, Takamatsu T: Remodeling of cell-cell and cell-extracellular matrix interactions at the border zone of rat myocardial infarcts. *Circ Res* 1999;85:1046-1055.